Data-Driven Analysis of High-Throughput Experiments on Liquid Battery Electrolyte Formulations: Unraveling the Impact of Composition on Conductivity

Anand Narayanan Krishnamoorthy[1], Christian Wölke[1], Diddo Diddens[1], Moumita Maiti[3], Youssef Mabrouk[1], Peng Yan[1], Mariano Grünebaum[1], Martin Winter[1,2], Andreas Heuer[1,3], Isidora Cekic-Laskovic[1*]*

[1] Forschungszentrum Jülich GmbH, Helmholtz-Institute Münster (IEK-12), Corrensstraße 46, 48149 Münster, Germany

[2] MEET Battery Research Center, University of Münster, Corrensstrasse 46, 48149 Münster, Germany

[3] Institute of Physical Chemistry, University of Münster, Corrensstrasse 28/30, 48149 Münster, Germany

Corresponding Authors

* Prof. Dr. Andreas Heuer: andheuer@uni-muenster.de

* Dr. Isidora Cekic-Laskovic: i.cekic-laskovic@fz-juelich.de

An in-house, unique, custom-developed high-throughput experimentation facility, used for discovery of novel and optimization of existing electrolyte formulations for diverse cell chemistries and targeted applications, follows a high-throughput formulation-characterization-performance-elucidation-optimization-evaluation chain based on a set of previously established requirements. Here, we propose a scalable data-driven workflow to predict ionic conductivities of non-aqueous battery electrolytes based on linear and Gaussian regression, considering a dataset acquired from one-of-a-kind high-throughput electrolyte formulation to high-throughput conductivity measurement sequence. Deeper insight into various compositional effects is gained from a generalized Arrhenius analysis, in which conductivities, activation energies and deviations from Arrhenius behavior are determined separately. Each observable displays a specific dependence on the electrolyte salt concentration. The conductivity is fully insensitive to the addition of electrolyte additives for otherwise constant molar composition. We also discuss and interpret qualitative trends predicted by the data-driven model in light of physical features such as viscosity or ion association effects.

TOC GRAPHICS
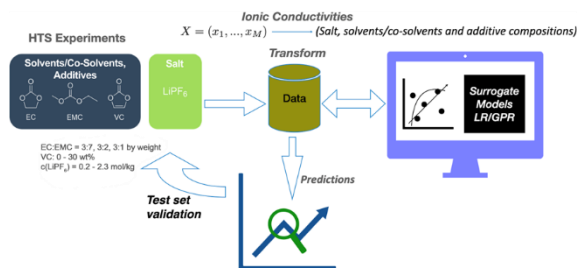
HIGH-THROUGHPUT EXPERIMENTATION: ELECTROLYTE FORMULATION AND CONDUCTIVITY MODULES

High-throughput (HT) strategies allow researchers to perform multiple experiments within a relatively short time in parallel rather than in sequence. Such strategies are generally achieved by using rapid automation tools including a large combination of material variables.[1–6] High-throughput experimentation (HTE) systems represent a highly valuable tool for accelerating the search towards advanced and optimized battery materials and with it, electrolyte formulations for given cell chemistry candidates, electrode-electrolyte interfaces, overall cell performance, safety and cost.[2] Recently, computational screening methodologies have been used to effectively support the battery material discovery process and a combinatorial approach of experiments and computational approach has been discussed as a way forward in the battery material discovery process.[7] Data driven models are predominantly used to extract knowledge and insights from noisy, structured and unstructured datasets.[8–10] Optimization of datasets (features, number of samples) are necessary to increase the efficiency of such models.[8,9,11,12] Currently artificial intelligence (AI) and machine learning algorithms are transforming material discovery processes, especially in battery science.[13]
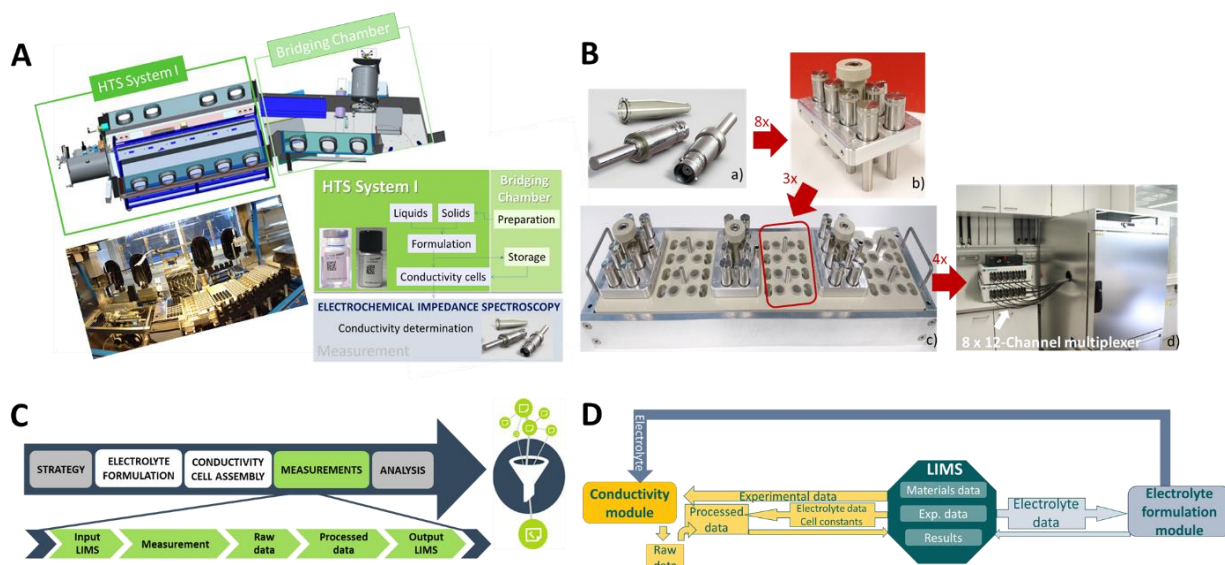
Figure 1. A) Electrolyte module featuring a fully automated HT system for electrolyte formulation and conductivity cell assembly with bridging chamber used for storage and preparation activities. B) Conductivity module comprising: a) in-house developed impedance electrode and Eppendorf tube b) small rack containing 8 electrodes c) big rack with 24 conductivity cells and d) potentiostat/galvanostat with 8 x 12-channel multiplexer and temperature chamber. C) Flow chart of fully automated electrolyte formulation to conductivity determination and analysis sequence. D) Schematic overview of the LIMS-modules interaction workflow.

The performance of all batteries (including Li-ion analogues) is governed by the nature of electrolytes used. The ionic conductivity in a liquid electrolyte, for instance co-determines the rate of the charging process. Organic solvent-based electrolyte formulations are of central relevance and still considered as state-of-the-art.[14,15] Common electrolyte formulations consist of lithium conducting salt such as lithium hexafluorophosphate ($LiPF_6$) and solvent mixtures comprising cyclic carbonates like ethylene carbonate (EC) and propylene carbonate (PC) with linear organic

carbonates like dimethyl carbonate (DMC), ethyl methyl carbonate (EMC) and diethyl carbonate (DEC) and provide desirable electrochemical properties for Li-ion batteries.[16–21]

Here we perform HT impedance spectroscopic experiments on $LiPF_6$-based electrolyte formulations containing EC and EMC as solvent mixture and vinylene carbonate (VC) as functional additive/co-solvent to determine ionic conductivities of resulting electrolyte formulations and develop a data driven model to predict ionic conductivities for variable electrolyte compositions. All data are extracted from HT experiments with conducting salt, solvent/co-solvent, additive compositions and temperature as features and ionic conductivity as target quantity. The electrolyte module of the HTE system, developed in-house, is composed of two independent, however well-connected units under a N_2 atmosphere (**Figure 1A**). Fully automated in nature, this HTE unit with a complex, however, user friendly configuration, conducts fast and systematic formulation of up to 96 different liquid electrolytes per working day, comprising a wide variety of lithium conducting salts, solvents/co-solvents and (multi)-functional additives as electrolyte components that can be combined with respect to their presence and amount in a considered electrolyte formulation. The robotic platform, providing a true HT workflow, was developed by combining multiple functionalities to an integrated platform system. It is composed of 21 stations enabling required gravimetric solid and liquid dispensing of selected electrolyte components with high accuracy (0.026% for solids and 0.024% for liquids), vial closing, vial mixing and heating and vial barcode labeling steps within the electrolyte formulation workflow (**Figure 1C**). A data matrix barcode contains all relevant information regarding the electrolyte composition and components like their amount, supplier, date of formulation and is easily readable by a smartphone app. The end-product is a cyclic olefin polymer vial, crimped with electrolyte resistant needle piercing septum or a screw cap aluminum vial and contains a maximum

10 mL of electrolyte formulation. Within the HTE unit, an automated filling of conductivity cells with electrolyte is performed as well. The second unit of the electrolyte module is the bridging chamber, fused for preparation and storage purposes, positioned in the glovebox under N_2 atmosphere.

For the electrolyte conductivity determination by means of electrochemical impedance spectroscopy (EIS), a conductivity module consisting of 96 measuring cells was developed. Considered electrolyte formulations were dispensed into disposable Eppendorf Safe-Lock Tubes in small sample quantities (750 µL) by the HTE robotic system in the glovebox under N_2 atmosphere. In-house developed electrodes were thereafter immersed in the electrolytes (**Figure1B(a)**). These electrodes as measuring probes deliver reproducible results regardless of the immersion depth in the electrolyte or the sample container geometry in the impedance measurements.[22] Eight conductivity cells were placed on a small rack (**Figure1B(b)**) and three of the small racks were positioned on a big rack (**Figure1B(c)**) for a total of 24 conductivity cells per big rack. Four big racks resulted in a total of 96 conductivity cells. To obtain the data on the internal resistance and conductivity of the electrolyte formulations, a Metrohm Autolab potentiostat/galvanostat with 8 x 12-channel multiplexer was used. The multiplexer, based on a particularly powerful single-board micro-controller, is capable of multiplexing each of the 12 potentiostat/galvanostat channels 8-fold, thus resulting in 96 controllable channels (**Figure1B(d)**). The assembled conductivity cells were placed in a temperature chamber with a 2 hour equilibration period for any given temperature prior to each measurement. Measurements were conducted in the temperature range from 0 °C to 60 °C in 10 °C increments. Once programmed with a temperature sequence, the setup requires no further user input.

Both electrolyte formulation and conductivity modules of the HTE facility are operated independently by a customized instance of the **L**aboratory **I**nformation **M**anagement **S**ystem (LIMS) adjusted to the specific system by the Quality Systems International (QSI) GmbH. The value chain, governed by the LIMS, is depicted in **Figure1D**. As the system's central entity, this software, flexible in nature, also serves as a material and data archive that ensures data provenance and enables backtracking of experiments. Materials data include specific identifiers (supplier, batch number, purity etc.) whereas experimental data consists of test protocols and relevant experimental parameters such as temperature. Besides saving the raw experimental data, the system is capable of processing the raw results and bundling them with relevant metadata (relevant details on the used electrolyte) into a machine-readable output format in order to provide users with all available information on a given experiment.

For the experiments reported in this work, the applied EC to EMC ratios were 3:7, 3:2 and 3:1 by weight with a VC content between 0 and 30 wt% with respect to EC and EMC. At the same time, the concentration of $LiPF_6$ was varied between 0.2 and 2.3 mol/kg. Exact amounts of all components for each electrolyte formulation can be found in the supporting information (SI - Table S1 and Table S2). Considering 7 different temperatures and repetition of each measurement for at least 3 times in respect to reproducibility for each electrolyte formulation, the total number of experimentally obtained data points amounted to 1200.

DATA DRIVEN ANALYSIS

For data analysis, a molar description of the electrolyte *via* $x_{LiPF6}\, LiPF_6 \cdot (1 - x_{LiPF6})[x_{VC}\, VC \cdot (1 - x_{VC})\, [x_{EC}\, EC \cdot (1 - x_{EC})\, EMC]]$ was used. In this representation, the EC/EMC ratio does not change under variation of the VC content, x_{VC}. The ranges were chosen to cover a broad section of the

composition space where feasible electrolyte formulations can be expected (i. e. homogeneous solutions). However, in some formulations with high EC and $LiPF_6$ content, crystal formation occurred, rendering these formulations unusable (see Figures S1-S5). NMR analysis revealed that the crystals taken from one of the formulations only consisted of $LiPF_6$ and EC, implying that the crystallizing compound is likely $Li(EC)_4PF_6$.[23] Some electrolyte formulations with low $LiPF_6$ and high EC content showed anomalous conductivity values at low temperatures, indicating freezing of EC in these cases (see Figure S5).

To provide a deeper understanding of HT datasets, conductivities are transformed according to the generalized Arrhenius fit ($X = (x_{LiPF6}, x_{VC}, x_{EC})$):

$$\log \sigma(X, T) = S_0(X) - S_1(X) * (\beta - \beta_0) - S_2(X) * (\beta - \beta_0)^2 \tag{1}$$

with the inverse onset temperature β_0. The surrogate models for the description of the $S_i(X)$ are formulated in terms of polynomials. The models as well as the choice of the order, also in the context of the available experimental data sets, is discussed in the methods section of SI. For the analysis we use dimensionless parameters. In particular, we choose $\beta = 1000/T$ where T is expressed in Kelvin [K]. These parameters have a direct interpretation: $exp[S_0(X)]$ corresponds to the conductivity at the onset temperature. The activation energy, evaluated at the onset temperature, is proportional to $S_1(X)$. Finally, $S_2(X)$ reflects possible deviations from pure Arrhenius behavior, showing up as a curvature. This transformation with implicit temperature description reduces the number of datasets and the corresponding parameters to 3 and all of them have a direct physical interpretation, providing additional information as compared to a polynomial fit of ionic conductivity.[24,25]

The choice of the onset temperature is obtained from the correlation of conductivity and activation energy at a given temperature. At low temperatures both quantities are strongly correlated, since high activation energies show very low conductivities at low temperatures and for the present set of electrolyte compositions this correlation diminishes at approximately 40 °C, as shown in the SI-Figure S7.
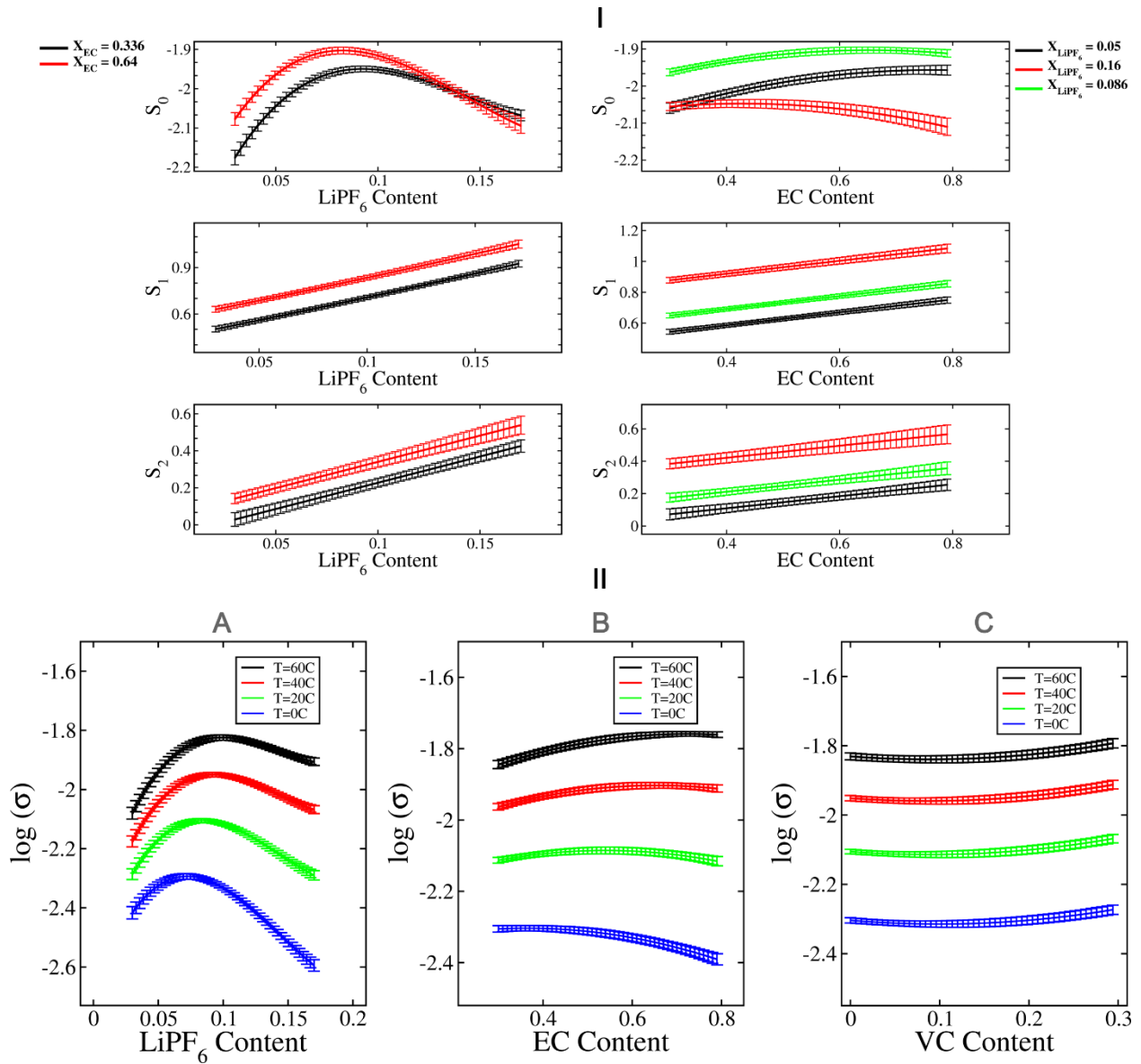

Figure 2. I) Predictions for the generalized Arrhenius fitting parameters $S_i(X)$ (S_0, S_1, S_2) with respect to x_{LiPF6} (left) and x_{EC} content (both for $x_{VC}=0.0$) (right). II) The change of ionic

conductivity with LiPF$_6$ content (A) for fixed [(x$_{VC}$=0.0, x$_{EC}$=0.336)] EC content (B) for fixed [(x$_{VC}$=0.0, x$_{LiPF6}$=0.086)] VC content (C) for fixed [(x$_{EC}$=0.336, x$_{LiPF6}$=0.087)] at different temperatures are shown below. All the results are shown for the LR model.

Here we use linear regression (LR) and Gaussian process regression (GPR) models to analyze the HT electrolyte conductivity datasets. GPR directly provides confidence intervals for the predictions, whereas for LR, we use a bootstrapping process to account for uncertainties in predictions.[8,26–30] The features are LiPF$_6$, VC, and EC concentrations and the predicted quantity is the logarithm of the ionic conductivity of the resulting electrolyte. Both LR (R^2 score - 0.986) and GPR (R^2 score - 0.987) show similar prediction accuracy for experimental ionic conductivities which to a large extent are determined by the experimental errors (see SI V.1)

The data driven workflow is independent of the nature of the dataset, thus can provide a leeway for larger dimensions of features like introduction of multiple co-solvent, additives or salt mixtures. This increased dimensionality of electrolyte formulations increases the complexity of empirical models which are generally used to interpret the relevance of electrolyte compositions on ionic conductivity.[24,25,31] Furthermore, data driven models provide robust error estimates of the predicted data, which are not provided by empirical fits.[8,24,25,32] Thus, these surrogate models provide an effective way to interpret acquired HT datasets independent of feature dimensions. Since both LR and GPR show similar results, we use LR to understand feature trends (x$_{LiPF6}$, x$_{VC}$, x$_{EC}$) on ionic conductivity in this letter for convenience. The trends with GPR are shown in SI Figure S13.

The conductivity at onset temperature $S_0(X)$ tends to increase with LiPF$_6$ content with a peak close to ~(0.07-0.09) and then drops for higher LiPF$_6$ content (**Figure 2 I**, left). A significant dependence on the EC content is observed. Starting from the low LiPF$_6$ content, the initial rise in electrolyte conductivity is typically attributed to an increasing number of dissociated ions per unit volume whereas the subsequent reduction of conductivity reflects the increasing viscosity. The presence of maximum conductivity values upon variation of the salt content has been observed for other lithium-based electrolytes as well.[24,25,31–35] In contrast, the activation energy term $S_1(X)$ and the curvature term $S_2(X)$ show a simple linear increase with increasing salt content. Higher values are observed for larger EC contents. Further, the resulting influence of temperature on the conductivity is shown in (**Figure 2 II A**). The peak of the conductivity shifts to higher LiPF$_6$ content with increasing temperature.

When analyzing the dependence on EC content, the ionic conductivity at the onset temperature increases with increasing EC content for lower LiPF$_6$ content ($x_{LiPF6} = 0.05$), whereas the trend reverses at higher salt content ($x_{LiPF6} = 0.16$). This directly shows the presence of significant LiPF$_6$ and EC content contributions to the conductivity at the onset temperature which furthermore are coupled (see SI Table S3). Thus, there is a strong impact of the LiPF$_6$ content on the EC dependent activation energy and curvature (**Figure 2 I**, right). Since the activation energy is just shifted, the impact is not coupled. Also, the dependence on the LiPF$_6$ concentration is more relevant for the transport properties than the replacement of EMC by EC and, e. g. the resulting variation of the dielectric constant.[36,37] Consistent with the properties of the activation energy in **Figure 2 I** right, the small peak in conductivity shifts to smaller values of the EC content at lower temperatures.[24]

Finally, the VC content does not play any role in bulk ionic conductivity for fixed EC/EMC ratio as shown in **Figure 2 II C** (see also SI Table S6). This is a remarkable result, given the similar

ring structure of EC and VC. However, VC is known to play a pivotal role in electrolyte|electrode interfacial interactions.[38,39]

In **Figure 3A**, the HTE obtained ionic conductivities, $\log(\sigma)$, for fixed EC/EMC ratio are compared with other experimental values for the conductivity. The results are compatible within the fluctuations. Furthermore, in **Figure 3B** we show the logarithm of the molar conductivities and in **Figure 3C** the activation energies, incorporating data for the viscosity[25,31] and binary diffusivity[25]. Remarkably, the logarithm of the molar conductivities (**Figure 3B**) as well as the activation energies (**Figure 3C**) basically display a linear behavior in the whole salt concentration regime which allows, e. g., a simple estimation of the maximum of the conductivity (estimations in **Figure 3A,** showing very good agreement), see SI V.6 for an explicit derivation. Thus, after removing the trivial impact of an increasing number of ions, there are no indications of changing mechanisms at the maximum. Furthermore, the salt dependence of the molar conductivity at fixed temperature as well as its activation energy is very similar to the respective observables, based on the viscosity. The remaining minor systematic deviations of the activation energies of the conductivity to the viscosity and diffusivity in **Figure 3C** indicate that the lowering of the conductivity as compared to the Nernst-Einstein prediction *via* pair formation is somewhat less pronounced for lower temperatures. The latter has been also reported for other systems.[40]
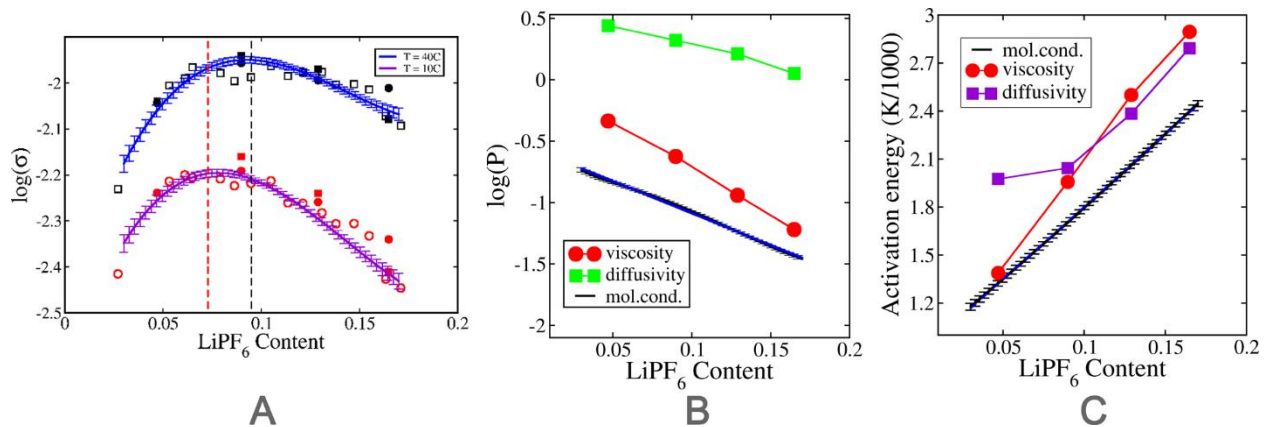
Figure 3. Comparison of different data for the 30:70 wt. EC:EMC system (no VC). (A) The LR conductivity in comparison to the data from Ref [31] (spheres) and Ref [25] (squares) at two different temperatures. The broken lines indicate the estimation of the maxima for both temperatures, based on the insight from (B) and (C). For details of the prediction process, see SI. (B) Comparison of the logarithm of different observables P as a function of salt content at T=25 °C. Specifically, we show the molar LR prediction of the molar conductivity σ/x, the viscosity [cP] from Ref [31] (spheres) and the diffusivity [$10^{-6}cm^2/s$] from Ref [25] (squares). Also included is a linear fit of the logarithm of the molar LR conductivity: $-0.56-5.21\,x_{LiPF6}$ (black); as broken line. Due to the excellent agreement with the molar conductivity data, it is hardly visible. (C) Comparison of the activation energies of the LR-based conductivity, the viscosity from Ref [31] and the diffusivity from Ref [25] for T=25 °C. The activation energy of the conductivity has been fitted by $0.89 + 9.1\,x_{LiPF6}$. The two latter activation energies have been estimated from the viscosity and diffusivity data at T=40 °C and T=10 °C from Ref [31], Ref [25,] respectively. The diffusivity data points at T=10 °C are estimated from interpolation of data at 12 °C and 2.5 °C as provided in Ref [25].

SUMMARY and OUTLOOK

The HT experimentation facility, in general, has the potential to predict a range of vital electrolyte properties and to establish a formulation-characterization-performance-elucidation-optimization evaluation chain. This involves the discovery of novel and the optimization of existing liquid electrolyte formulations for diverse cell chemistries by using a filtration effect based on the previously established set of requirements for a targeted application. From a first round of preselected, automated experiments[3–5,41–43], lead/hit candidates can be selected and characterized further in subsequent steps. The resulting optimization process may involve the chosen concentrations or the use of different components.

In summary, we propose an in-house developed HT approach to conduct automated impedance experiments in parallel for different electrolyte formulation to attain optimal ionic conductivities. This approach reduces considerably the amount of time required for performing experiments manually and enables accelerated electrolyte discovery process for battery applications. Data driven models, based, in this case, on 1200 experimentally acquired data points, are used to analyze and predict ionic conductivities and can further be used to automatically identify outliers and thus increase the robustness of HT experiments. It is shown that these surrogate models predict ionic conductivities close to experimental accuracies and provide reliable estimates at very low cost compared to actual experiments. Also the flexibility of the surrogate models with regard to statistical uncertainties provides an effective way to study feature trends on ionic conductivity compared to standard empirical models. The transformed data driven model provides a physical interpretation of trends of electrolyte compositions on ionic conductivity. Furthermore, via additional microscopic simulations, performed in parallel to the experiments, important physical and chemical additional insight can be gained. This may complement the results from experiments

and data driven model, thereby obtaining a holistic understanding of relevant electrolyte formulations.

ASSOCIATED CONTENT

Supporting Information Available: Electrolyte compositions, GPR results, additional details on data-driven analysis

AUTHOR INFORMATION

Dr. Anand Narayanan Krishnamoorthy: k.anand.narayanan@fz-juelich.de

Dr. Christian Wölke: c.woelke@fz-juelich.de

Dr. Diddo Diddens: d.diddens@fz-juelich.de

Dr. Moumita Maiti: maiti@uni-muenster.de

Youssef Mabrouk: y.mabrouk@fz-juelich.de

Peng Yan: p.yan@fz-juelich.de

Dr. Mariano Grünebaum: m.gruenebaum@fz-juelich.de

Prof. Dr. Martin Winter: martin.winter@uni-muenster.de

* Prof. Dr. Andreas Heuer: andheuer@uni-muenster.de

* Dr. Isidora Cekic-Laskovic: i.cekic-laskovic@fz-juelich.de

Notes

The authors declare no competing financial interest.

REFERENCES

(1)   Shevlin, M. Practical High-Throughput Experimentation for Chemists. *ACS Med. Chem. Lett.* **2017**, *8* (6), 601–607. https://doi.org/10.1021/acsmedchemlett.7b00165.

(2)   Hahn, R.; Ferch, M.; Tribowski, K.; Kyeremateng, N. A.; Hoeppner, K.; Marquardt, K.; Lang, K.-D.; Bock, W. High-Throughput Battery Materials Testing Based on Test Cell Arrays and Dispense/Jet Printed Electrodes. *Microsyst. Technol.* **2019**, *25* (4), 1137–1149. https://doi.org/10.1007/s00542-019-04368-5.

(3)   Benz, M.; Asperger, A.; Hamester, M.; Welle, A.; Heissler, S.; Levkin, P. A. A Combined High-Throughput and High-Content Platform for Unified on-Chip Synthesis, Characterization and Biological Screening. *Nat. Commun.* **2020**, *11*, 5391. https://doi.org/10.1038/s41467-020-19040-0.

(4)   Blow, N. High-Throughput Screening: Designer Screens. *Nat. Methods* **2009**, *6*, 105–108. https://doi.org/10.1038/nmeth0109-105.

(5)   Chakraboty, S.; Xie, W.; Mathews, N.; Sherburne, M.; Ahuja, R.; Asta, M.; Mhaisalkar, S. G. Rational Design: A High-Throughput Computational Screening and Experimental Validation Methodology for Lead-Free and Emergent Hybrid Perovskites. *ACS Energy Lett.* **2017**, *2* (4), 837–845. https://doi.org/10.1021/acsenergylett.7b00035.

(6)   DiLuzio, S.; Mdluli, V.; U Connel, T.; Lewis, J.; VanBenschoten, V.; Bernhard, S. High-Throughput Screening and Automated Data-Driven Analysis of the Triplet Photophysical Properties of Structurally Diverse, Heteroleptic Iridium(III) Complexes. *JACS* **2021**, *143* (2), 1179–1194. https://doi.org/10.1021/jacs.0c12290.

(7)   Cheng, L.; Assary, R. S.; Qu, X.; Jain, A.; Ong, S. P.; Rajput, N. N.; Persson, K.; Curtiss, L. A. Accelerating Electrolyte Discovery for Energy Storage with High-Throughput Screening. *J. Phys. Chem. Lett.* **2015**, *6* (2), 283–291. https://doi.org/10.1021/jz502319n.

(8)   Schmidt, J.; Marques, M. R. G.; Botti, S.; Marques, M. A. L. Recent Advances and Applications of Machine Learning in Solid-State Materials Science. *Npj Comput. Mater.* **2019**, *5* (1), 83. https://doi.org/10.1038/s41524-019-0221-0.

(9)   Li, Y.; Liu, K.; Foley, A. M.; Zulke, A.; Berecibar, M.; Nanini Maury, E.; Mierlo Joeri Van; Hoster, H. E. Data-Driven Health Estimation and Lifetime Prediction of Lithium-Ion Batteries: A Review. *Renew. Sustain. Energy Rev.* *113*, 109254. https://doi.org/10.1016/j.rser.2019.109254.

(10) Eslamloueyan, R.; Khademi, M. H.; Mazinani, S. Using a Multilayer Perceptron Network for Thermal Conductivity Prediction of Aqueous Electrolyte Solutions. *Ind Eng Chem Res* **2011**, *50* (7), 4050–4056. https://doi.org/doi.org/10.1021/ie101513z.

(11) Sivaraman, G.; Krishnamoorthy, A. N.; Baur, M.; Holm, C.; Stan, M.; Csányi, G.; Benmore, C.; Vázquez-Mayagoitia, Á. Machine-Learned Interatomic Potentials by Active Learning: Amorphous and Liquid Hafnium Dioxide. *Npj Comput. Mater.* **2020**, *6* (1), 1–8. https://doi.org/10.1038/s41524-020-00367-7.

(12) Sivaraman, G.; Gallington, L.; Krishnamoorthy, A. N.; Stan, M.; Csányi, G.; Vázquez-Mayagoitia, Á.; Benmore, C. J. Experimentally Driven Automated Machine-Learned Interatomic Potential for a Refractory Oxide. *Phys. Rev. Lett.* **2021**, *126* (15), 156002. https://doi.org/10.1103/PhysRevLett.126.156002.

(13) Benayad, A.; Diddens, D.; Heuer, A.; Krishnamoorthy, A. N.; Maiti, M.; Cras, F. L.; Legallais, M.; Rahmanian, F.; Shin, Y.; Stein, H.; Winter, M.; Wölke, C.; Yan, P.; Cekic-Laskovic, I. High-Throughput Experimentation and Computational Freeway Lanes for Accelerated Battery Electrolyte and Interface Development Research. *Adv. Energy Mater.* **2021**, 2102678. https://doi.org/10.1002/aenm.202102678.

(14) Karatrantos, A. V.; Khan, M. S.; Yan, C.; Dieden, R.; Urita, K.; Ohba, T.; Cai, Q. Ion Transport in Organic Electrolyte Solutions for Lithium-Ion Batteries and Beyond. *J. Energy Power Technol. - LiDSEN* **2021**, *3* (3). https://doi.org/doi:10.21926/jept.2103043.

(15) Winter, M.; Barnett, B.; Xu, K. Before Li Ion Batteries. *Chem. Rev.* **2018**, *118* (23), 11433–11456. https://doi.org/10.1021/acs.chemrev.8b00422.

(16) Xu, K. Nonaqueous Liquid Electrolytes for Lithium-Based Rechargeable Batteries. *Chem. Rev.* **2004**, *104* (10), 4303–4418. https://doi.org/10.1021/cr030203g.

(17) Borodin, O.; Smith, G. D. Quantum Chemistry and Molecular Dynamics Simulation Study of Dimethyl Carbonate: Ethylene Carbonate Electrolytes Doped with $LiPF_6$. *J. Phys. Chem. B* **2009**, *113* (6), 1763–1776. https://doi.org/10.1021/jp809614h.

(18) Oldiges, K.; Diddens, D.; Ebrahiminia, M.; Hooper, J. B.; Cekic-Laskovic, I.; Heuer, A.; Bedrov, D.; Winter, M.; Brunklaus, G. Understanding Transport Mechanisms in Ionic Liquid/Carbonate Solvent Electrolyte Blends. *Phys. Chem. Chem. Phys.* **2018**, *20* (24), 16579–16591. https://doi.org/10.1039/C8CP01485J.

(19) Borodin, O.; Olguin, M.; Ganesh, P.; Kent R C, P.; Allen, J. L.; Henderson, W. A. Competitive Lithium Solvation of Linear and Cyclic Carbonates from Quantum Chemistry. *Phys. Chem. Chem. Phys.* **2016**, *18* (1), 164–175. https://doi.org/10.1039/C5CP05121E.

(20) Ong, T. M.; Verners, O.; Draeger W, E.; van Duin C T, A.; Lordi, V.; Pask, J. E. Lithium Ion Solvation and Diffusion in Bulk Organic Electrolytes from First-Principles and Classical Reactive Molecular Dynamics. *J. Phys. Chem. B* **2015**, *119* (4), 1535–1545. https://doi.org/10.1021/jp508184f.

(21) Cekic-Laskovic, I.; von Aspern, N.; Imholt, L.; Kaymaksiz, S.; Oldiges, K.; Rad, B. R.; Winter, M. Synergistic Effect of Blended Components in Nonaqueous Electrolytes for Lithium Ion Batteries. *Top. Curr. Chem.* **2017**, *375* (2), 37. https://doi.org/10.1007/s41061-017-0125-8.

(22) Hans-Dieter Wiemhöfer; Mariano Grünebaum; Martin Manuel Hiller. MICRO ELECTRODE LIQUID MEASUREMENT CELL. WO 2014/139494 A1, September 18, 2014.

(23) Zavalij, P. Y.; Yang, S.; Wittingham, M. S. CCDC 244695: Experimental Crystal Structure Determination. **2005**. https://doi.org/10.5517/cc86mdg.

(24) M S, D.; Xu, K.; Zhang, S.; Amine, K.; Henriksen, G. L.; Jow, R. Change of Conductivity with Salt Content, Solvent Composition, and Temperature for Electrolytes of $LiPF_6$ in Ethylene Carbonate-Ethyl Methyl Carbonate. *J. Electrochem. Soc. 148* (10), A1196-1204. https://doi.org/10.1149/1.1403730.

(25) Landesfeind, J.; Gasteiger, H. A. Temperature and Concentration Dependence of the Ionic Transport Properties of Lithium-Ion Battery Electrolytes. *J. Electrochem. Soc.* **2019**, *166* (14), A3079–A3097. https://doi.org/10.1149/2.0571912jes.

(26) Rasmussen, C. E.; Williams, C. K. I. *Gaussian Processes for Machine Learning*; Adaptive computation and machine learning; MIT Press: Cambridge, Mass, 2006.

(27) Duvenaud, D. K. Automatic Model Construction with Gaussian Processes, University of Cambridge, 2014.

(28) Fomenko, I.; Durst, M.; Balaban, D. Robust Regression for High Throughput Drug Screening. *Comput. Methods Programs Biomed.* **2006**, *82* (1), 31–37. https://doi.org/10.1016/j.cmpb.2006.01.008.

(29) Eck, D. Bootstrapping for Multivariate Linear Regression Models. *Stat. Probab. Lett.* **2017**, *134*. https://doi.org/10.1016/j.spl.2017.11.001.

(30) Fox, J. Bootstrapping Regression Models. https://artowen.su.domains/courses/305-1314/FoxOnBootingRegInR.pdf 2002.

(31) Logan, E. R.; Tonita, E. M.; Gering, K. L.; Li, J.; Ma, X.; Beaulieu, L. Y.; Dahn, J. R. A Study of the Physical Properties of Li-Ion Battery Electrolytes Containing Esters. *J. Electrochem. Soc.* **2018**, *165* (2), A21–A30. https://doi.org/10.1149/2.0271802jes.

(32) Solchenbach, S.; Metzger, M.; Egawa, M.; Beyer, H.; Gasteiger, H. A. Quantification of PF_5 and POF_3 from Side Reactions of $LiPF_6$ in Li-Ion Batteries. *J. Electrochem. Soc.* **2018**, *165* (13), A3022–A3028. https://doi.org/: 10.1149/2.0481813jes.

(33) Chen, H. P.; Fergus, J. W.; Jang, B. Z. The Effect of Ethylene Carbonate and Salt Concentration on the Conductivity of Propylene Carbonate|Lithium Perchlorate Electrolytes. *J. Electrochem. Soc.* **2000**, *142* (2), 399–406.

(34) Narayanan Krishnamoorthy, A.; Oldiges, K.; Winter, M.; Heuer, A.; Laskovic, I. C.; Holm, C.; Smiatek, J. Electrolyte Solvents for High Voltage Lithium Ion Batteries: Ion Correlation and Specific Anion Effects in Adiponitrile. *Phys. Chem. Chem. Phys.* **2018**, *20* (40), 25701–25715. https://doi.org/10.1039/C8CP04102D.

(35) Xu, K.; Lam, Y.; Zhang, S. S.; Jow, T. R.; Curtis, T. B. Solvation Sheath of Li^+ in Nonaqueous Electrolytes and Its Implication of Graphite/Electrolyte Interface Chemistry. *J. Phys. Chem. C* **2007**, *111* (20), 7411–7421. https://doi.org/10.1021/jp068691u.

(36) Valøen, L. O.; Reimers, J. N. Transport Properties of $LiPF_6$-Based Li-Ion Battery Electrolytes. *J. Electrochem. Soc.* **2005**, *152* (5), A882. https://doi.org/10.1149/1.1872737.

(37) Nyman, A.; Behm, M.; Lindbergh, G. Electrochemical Characterisation and Modelling of the Mass Transport Phenomena in $LiPF_6$–EC–EMC Electrolyte. *Electrochimica Acta* **2008**, *53* (22), 6356–6365. https://doi.org/10.1016/j.electacta.2008.04.023.

(38) Aurbach, D.; Gamolsky, K.; Markovsky, B.; Gofer, Y.; Schmidt, M.; Heider, U. On the Use of Vinylene Carbonate (VC) as an Additive to Electrolyte Solutions for Li-Ion Batteries. *Electrochimica Acta* **2002**, *47* (9), 1423–1439. https://doi.org/10.1016/S0013-4686(01)00858-1.

(39) Qian, Y.; Schultz, C.; Niehoff, P.; Schwieters, T.; Nowak, S.; Schappacher, F. M.; Winter, M. Investigations on the Electrochemical Decomposition of the Electrolyte Additive Vinylene Carbonate in Li Metal Half Cells and Lithium Ion Full Cells. *J. Power Sources* **2016**, *332*, 60–71. https://doi.org/10.1016/j.jpowsour.2016.09.100.

(40) Walz, M.-M.; van der Spoel, D. Microscopic Origins of Conductivity in Molten Salts Unraveled by Computer Simulations. *Commun. Chem.* **2021**, *4* (9). https://doi.org/10.1038/s42004-020-00446-2.

(41) Makarenkov, V.; Kevorkov, D.; Zentilli, P.; Gagarin, A.; Malo, N.; Nadon, R. HTS-Corrector: Software for the Statistical Analysis and Correction of Experimental High-Throughput Screening Data. *Bioinformatics* **2006**, *22* (11), 1408–1409. https://doi.org/doi.org/10.1093/bioinformatics/btl126.

(42) Rein, J.; Annand, J. R.; Wismer, M. K.; Fu, J.; C Siu, J.; Klapars, A.; Strotman, N. A.; Kalyani, D.; Lehnherr, D.; Lin, S. Unlocking the Potential of High-Throughput Experimentation for Electrochemistry with a Standardized Microscale Reactor. *ACS Cent. Sci.* **2021**, *7* (8), 1347–1355. https://doi.org/doi.org/10.1021/acscentsci.1c00328.

(43) Matsuda, S.; Nishioka, K.; Nakanishi, S. High-Throughput Combinatorial Screening of Multi-Component Electrolyte Additives to Improve the Performance of Li Metal Secondary Batteries. *Sci. Rep.* **2019**, *9* (1), 6211. https://doi.org/10.1038/s41598-019-42766-x.